

SMOOTH H I LOW COLUMN DENSITY OUTSKIRTS IN NEARBY GALAXIES

R. IANJAMASIMANANA¹, FABIAN WALTER¹, W.J.G. DE BLOK^{2,3,4}, GEORGE H. HEALD^{5,4}, ELIAS BRINKS⁶
(Accepted for Publication in the *Astronomical Journal*)

¹Max-Planck Institut für Astronomie, Königstuhl 17, 69117, Heidelberg, Germany

²Netherlands Institute for Radio Astronomy (ASTRON), Postbus 2, 7990 AA Dwingeloo, The Netherlands

³Astrophysics, Cosmology and Gravity Centre, Department of Astronomy, University of Cape Town, Private Bag X3, Rondebosch 7701, South Africa

⁴Kapteyn Astronomical Institute, University of Groningen, PO Box 800, 9700 AV, Groningen, The Netherlands

⁵CSIRO Astronomy and Space Science, 26 Dick Perry Avenue, Kensington WA 6151, Australia

⁶Centre for Astrophysics Research, University of Hertfordshire, College Lane, Hatfield, AL10 9AB, UK

ABSTRACT

The low column density gas at the outskirts of galaxies as traced by the 21 cm hydrogen line emission (H I) represents the interface between galaxies and the intergalactic medium, i.e., where galaxies are believed to get their supply of gas to fuel future episodes of star formation. Photoionization models predict a break in the radial profiles of H I at a column density of $\sim 5 \times 10^{19} \text{ cm}^{-2}$ due to the lack of self-shielding against extragalactic ionizing photons. To investigate the prevalence of such breaks in galactic disks and to characterize what determines the potential *edge* of the H I disks, we study the azimuthally-averaged H I column density profiles of 17 nearby galaxies from The H I Nearby Galaxy Survey (THINGS) and supplemented in two cases with published Hydrogen Accretion in LOcal GALaxieS (HALOGAS) data. To detect potential faint H I emission that would otherwise be undetected using conventional moment map analysis, we line up individual profiles to the same reference velocity and average them azimuthally to derive stacked radial profiles. To do so, we use model velocity fields created from a simple extrapolation of the rotation curves to align the profiles in velocity at radii beyond the extent probed with the sensitivity of traditional integrated H I maps. With this method, we improve our sensitivity to outer-disk H I emission by up to an order of magnitude. Except for a few disturbed galaxies, none show evidence for a sudden change in the slope of the H I radial profiles, the alleged signature of ionization by the extragalactic background.

Keywords: galaxies: evolution – galaxies: halos – galaxies: ISM – radio lines: ISM

1. INTRODUCTION

The 21 cm atomic hydrogen (H I) line can trace the interstellar medium (ISM) out to large radii in galaxies (e.g., [Bosma 1981](#)), typically well beyond the optical disk. Detailed studies of the shapes of the radial H I distribution are important to understand the physical conditions of the outer disk of galaxies, e.g., constrain models of the H I to H II transition, to trace the influence of environment on H I, and to use the H I gas as a tracer of the (dark) matter distribution. In general, the radial H I distribution tends to be approximately flat out to about the edge of the optical disk (with a central de-

pression for many spiral galaxies), followed by a gradual decline (e.g., early work by [Sancisi 1983](#); [Broeils & van Woerden 1994](#)) at a column density of about a few times 10^{20} cm^{-2} . A second break in the radial H I profiles has been reported using high sensitivity observations of M33 ([Corbelli et al. 1989](#)) and NGC 3198 ([van Gorkom 1993](#)). In these studies, a break was reported at a column density of a few times 10^{19} cm^{-2} . Such a behavior has been interpreted in the context of the existence of a critical column density below which H I is ionized by the extragalactic radiation field ([Corbelli & Salpeter 1993](#); [Maloney 1993](#); [Dove & Shull 1994](#)). However, as mentioned by [Irwin \(1995\)](#), the degree of steepness of the radial H I fall-off predicted by ionization models depends on many factors such as the vertical structure of the H I disk, the H I mass distribution, and more importantly the flux of the ionizing photons, which are not well constrained by observations (see also [Dove & Shull 1994](#); [Fumagalli et](#)

ianjamasimanana26@gmail.com
walter@mpia.de
blok@astron.nl
George.Heald@csiro.au
e.brinks@herts.ac.uk

al. 2017).

Although there have been many discussions in the literature explaining the edge of the H I disk from theoretical viewpoints (Sunyaev 1969; Bergeron & Gunn 1977; Bosma 1981; Corbelli & Salpeter 1993; Maloney 1993; Dove & Shull 1994), detailed observations of the radial extent of the outer H I disk in a sample of galaxies are lacking.

Using single-dish observations with the Arecibo telescope, Corbelli et al. (1989) examined the outer radial H I distribution of the northern part of the major axis of M33 down to a (3σ detection limit) column density of $\sim 2 \times 10^{18} \text{ cm}^{-2}$. The column density is $\sim 2 \times 10^{21} \text{ cm}^{-2}$ in the central disk and the value drops below $\sim 2 \times 10^{20} \text{ cm}^{-2}$ just outside the optical disk, which then gradually declined to $\sim 3 \times 10^{19} \text{ cm}^{-2}$. A second break in the radial profile was observed at $\sim 3 \times 10^{19} \text{ cm}^{-2}$, below which the value decreased to $\sim 2 \times 10^{18} \text{ cm}^{-2}$ within $\sim 1 \text{ kpc}$. The NRAO¹ Very Large Array (VLA) observation of NGC 3198 by van Gorkom (1993), with a 3σ column density limit of $4 \times 10^{18} \text{ cm}^{-2}$, also revealed the existence of a radial break of the H I disk below $\sim 2 \times 10^{19} \text{ cm}^{-2}$. The VLA data showed that the H I surface density of NGC 3198 decreased by an order of magnitude from ~ 30 to $\sim 33 \text{ kpc}$. The abrupt decline in NGC 3198 was, however, not resolved within the synthesized beam of the observation ($\sim 2.7 \text{ kpc}$). Recently Heald et al. (2016) studied the H I edge in M83 using interferometric observations with the Karoo Array Telescope (KAT-7, a 7 dish radio telescope in South Africa, precursor to the MeerKAT telescope; Carignan et al. 2013). These observations reached a 3σ column density sensitivity of $5.6 \times 10^{18} \text{ cm}^{-2}$. Based on the analysis of the H I column density map of M83, they concluded that this galaxy also has an H I edge similar to what was found for NGC 3198 and M33. Heald et al. (2016) considered ram pressure or ionization by the intergalactic medium as a possible cause of the H I edge. There are also other observations targeting the H I outskirts of nearby galaxies (e.g., Irwin et al. 2009) but we restrict ourselves to those that specifically address the edge of the H I disk.

In this paper, we study the shapes of the radial H I column density profiles for a large sample of nearby galaxies and investigate whether the presence of an edge is a common feature of the H I disk. We do this by employing a new method to extract faint H I emission at large galactocentric radii from H I data cubes. Our paper is organized as follows. In Section 2, we present our

data and sample galaxies. In Section 3, we describe our new stacking approach to derive the radial H I column density profiles. In Section 4, we discuss our results. In Section 5, we present our summary and conclusions.

2. DATA AND SAMPLE

Analyzing the distribution of the H I emission at large radii requires high sensitivity observations. With the limitation of current state-of-the-art telescopes, only observations of nearby galaxies provide enough spatial resolution and sensitivity to resolve the H I edge and investigate the H I distribution at large radii. Based on the model by Maloney (1993) and the previous study of NGC 3198 by van Gorkom (1993), a column density sensitivity limit of $\sim 10^{19} \text{ cm}^{-2}$ and a spatial resolution better than 2.7 kpc are required to detect and resolve the H I edge. Using a stacking method that will be described later, we satisfy this criteria using data from The H I Nearby Galaxy Survey (THINGS; Walter et al. 2008). THINGS provides VLA 21-cm line maps of 34 nearby spiral and dwarf galaxies at an average angular resolution of $\sim 11''$ (linear resolution is given in Table 1).

Table 1. The Sample galaxies

Galaxy	incl	Dist.	B _{min}	B _{maj}	Lin. res.
1	[°]	[Mpc]	['']	['']	[pc]
IC 2574	53	4.0	11.9	12.8	240
NGC 3621	65	6.6	10.2	15.9	419
NGC 2366	64	3.4	11.8	13.1	206
DDO 154	66	4.3	12.6	14.1	278
NGC 6946	33	5.9	5.6	6.0	167
NGC 4736	41	4.7	9.1	10.2	220
NGC 3521	73	10.7	11.2	14.1	656
NGC 4826	65	7.5	9.3	12.2	391
NGC 3627	62	9.3	8.8	10.6	438
NGC 925	66	9.2	5.7	5.9	260
NGC 3198	72	9.4	11.6	13.0	560
NGC 7331	76	14.7	5.6	6.1	418
NGC 2841	74	14.1	9.4	11.1	698
NGC 2403	63	3.2	7.7	8.8	127
NGC 2903	65	8.9	13.3	15.3	617
NGC 7793	50	3.9	10.8	15.6	250
NGC 2976	65	3.6	6.4	7.4	121

NOTE—Column 1: name of galaxy; Column 2: inclination; Column 3: distance; Column 4&5: minor and major axes of synthesized beam in arcsec using a natural weighting; Column 6: average linear resolution.

In this work, we use the high resolution rotation curves derived by de Blok et al. (2008) (see Section 3). Thus we require that our galaxies are part of the de Blok et

¹ The National Radio Astronomy Observatory is a facility of the National Science Foundation operated under cooperative agreement by Associated Universities, Inc.

al. (2008) sample. However, we exclude NGC 5055 as this galaxy is strongly warped. We also exclude M81 as its HI emission is heavily disturbed, due to its interaction with M82 and NGC 3077. Thus, our sample is reduced to 17 spiral and dwarf galaxies. Their observational properties and names are shown for reference in Table 1 (see also Walter et al. 2008).

In this paper, we use the THINGS natural-weighted data and do not apply any residual flux correction nor blanking so that we preserve the noise properties of the data. However, to remove the flux discrepancy due to the mismatch between the shapes of the dirty beam and the restoring clean beam (for a full discussion, see Walter et al. 2008), we clean the data close to the noise level (1.5σ , as opposed to the 2.5σ of the standard THINGS data release). When cleaning to this depth, we find better agreement between the flux derived from the natural non-residual scaled cubes and the flux from the standard THINGS moment zero maps, which were derived from residual-scaled cubes (see also Ianjamasimanana et al. 2017). For completeness, we also present in this paper the radial HI column density profiles derived from the standard THINGS moment zero maps.

A few of the THINGS galaxies have also been observed as part of the Hydrogen Accretion in LOcal GALaxieS Survey (HALOGAS; Heald et al. 2011). For two galaxies (NGC 3198 and NGC 2403) which overlap with the HALOGAS sample and fulfill our sample selection criterion, we compare our results from the THINGS data with those from the HALOGAS data. HALOGAS is a deep HI survey of 24 nearby galaxies, with 23 galaxies observed by the WSRT² (Oosterloo et al. 2007; Heald et al. 2011) and one by the VLA (Fraternali et al. 2002). The WSRT data by Heald et al. (2011) have a typical (5σ per 4.1 km s^{-1} channel) column density sensitivity limit of $\sim 5 \times 10^{18} \text{ cm}^{-2}$ at $30''$ resolution using a Briggs’s (Briggs 1995) robustness parameter of 0 with a Gaussian taper. The VLA data (NGC 2403) by Fraternali et al. (2002) reached a (5σ per 5.2 km s^{-1} channel) column density sensitivity of $\sim 5 \times 10^{19} \text{ cm}^{-2}$ using a Robust (robust = 0.2) or Briggs weighting scheme at $15''$ (230 pc) angular resolution.

3. METHODOLOGY

We aim to derive HI column density values as a function of radius, beyond the extent probed by conventional pixel-by-pixel moment map analysis. To do so, we divide each galaxy into concentric elliptical annuli, each of them with a width along the major axis similar to the size of the synthesized beam of the observations. For THINGS and the VLA data from Fraternali et al.

(2002), we adopt a common width of $15''$; for the HALOGAS data of NGC 3198, we use a $30''$ width. Using a stacking technique that will be described in the next section, we derive the average HI column density within each annulus to derive the radial profiles. Since we aim to recover HI flux out to large radii, correction for sensitivity bias due to the response of the primary beam of the telescope is important. We therefore apply a primary beam correction in the analysis that follows.

3.1. Stacking of HI spectra

Detecting HI emission in the extreme outskirts of galaxies is challenging due to the low signal-to-noise (S/N) of the individual profiles. We here aim to push the sensitivity limit of the available HI data to much deeper levels. To do so, we stack and sum individual profiles within the elliptical annuli mentioned in the previous section to get high S/N azimuthally averaged HI profiles. Individual profiles at different positions within a data cube peak at different velocities predominantly due to the rotation of the gas within the galaxy disk. Consequently, they cannot be simply summed or averaged but individual spectra need to be aligned to a common reference velocity prior to the averaging. Faint HI emission that would otherwise be undetected (or “blanked”) using conventional pixel-by-pixel moment map analysis can thus be recovered. We therefore shift individual profiles by the amount suggested by the galaxy’s velocity field to attempt to align them to the same velocity (Ianjamasimanana et al. 2012). This technique is implemented in the GIPSY³ task SHUFFLE. The stacking is straightforward in the bright inner disk of galaxies, where the velocity fields are well determined (for a full discussion of the derivation of the THINGS velocity fields, see de Blok et al. 2008). However, in the faint outskirts of the disks, where the peak emission of the individual profiles falls below 3 times the rms noise, direct measurements of the velocity field cannot be derived. At such large radii, we will use extrapolations of the rotation curves derived in the inner disk by de Blok et al. (2008) to create model velocity fields. As most galaxies reach the flat part of the rotation curve at large radii, we here simply assume that the rotation curve will continue to stay flat beyond the last point where the rotation curves can be directly measured. We also assume that the position angle and inclination remain constant as well, i.e., there is no warp beyond the outermost radius directly detected in HI emission. These assumptions are the key elements of our stacking procedure. As we will see below, stacked HI signal is recovered be-

² Westerbork Synthesis Radio Telescope

³ The Groningen Image Processing System, <https://www.astro.rug.nl/~gipsy/articles/gipsypaper.html>

yond the measured rotation curves, which implies that the assumption of flat, extended rotation curves holds.

3.2. Effects of noisy profiles

Since we are stacking profiles azimuthally, we are summing both low and high S/N profiles. We thus assign a weight, w_i , to each individual profile or spectrum, S_i , before the stacking. We assume that the noise in the data cubes is uniform before the primary beam correction. This is a good assumption for our data cubes. After the primary beam correction, the noise is no longer uniform and we define our stacked profiles as

$$S = \frac{\sum_{i=1}^N w_i S_i}{\sum_{i=1}^N w_i}, \quad (1)$$

where $w_i = \frac{p_i^2}{\sigma_i^2}$ is the weight assigned to spectrum S_i , with p_i being the associated primary beam correction factor (we adopt a Gaussian shape, with $p_i = 1$ at the center and 0.5 at 15.4' and 17.0' from the pointing center of the VLA and WSRT, respectively) and σ_i is the rms noise before the correction. Since σ_i is assumed to be equal to σ for all profiles in a data cube, Equation 1 becomes

$$S = \frac{\sum_{i=1}^N p_i^2 S_i}{\sum_{i=1}^N p_i^2}. \quad (2)$$

We use a simple propagation of errors to define the noise of the stacked profiles in each elliptical annulus. Some stacked profiles show negative bowls due to unsampled (u , v) data (i.e., ‘‘missing short spacings’’). We correct for this by fitting a single or double Gaussian function with a polynomial background to the stacked profiles. We then convert the integrated flux of the fitted Gaussian components with respect to the fitted baseline to a column density. Finally, to correct for the orientation of the galaxies, we multiply the results by the cosine of the inclination of the galaxies to derive the actual surface density profiles. The adopted inclination values are listed in Table 1.

4. RESULTS

4.1. Examples of azimuthally stacked spectra

In Figure 1 we show examples of the azimuthally averaged stacked profiles of NGC 7331, derived using the model velocity field obtained from the model rotation curve shown as the blue solid line in the figure. We show the profiles for all sample galaxies in Figure A1 of the Appendix. In the region where the rotation curve is defined, we fit the rotation curve with a spline function.

Beyond this, we assume a flat rotation curve. We derive extended model velocity fields from the model rotation curves and use them as inputs for the stacking method implemented in the GIPSY task SHUFFLE. Note that if our estimate of the rotation curves significantly deviates from the *true* rotation curves, we would not be able to detect a signal. Figure 1 demonstrates that we are indeed able to detect signal beyond what is reached by conventional pixel-by-pixel analysis. The outermost point of the observed rotation curve measured by de Blok et al. (2008) is at $\sim 350''$ (using a 3σ cut-off) but we are able to still detect stacked HI emission out to a radius of $\sim 530''$. The fairly constant width of the profiles indicates that our assumption of a flat rotation curve is reasonable. The profiles remain narrow and we do not see multiple peaked or broad profiles as would be expected from an incorrect shift of the individual velocity profiles. There is a shift away from ‘zero’ velocities, though. This shift is the consequence of the northern side of NGC 7331 having slightly more HI emission than the southern side.

4.2. Radial profiles for all galaxies

In Figure 2, we show the radial column density profiles of the sample galaxies as derived using our stacking method. Out of the 17 galaxies studied, we reach a column density sensitivity limit of $\sim 10^{19} \text{ cm}^{-2}$ for 9 galaxies, and below $\sim 10^{19} \text{ cm}^{-2}$ for 8 galaxies. As a check, we also show the radial column density profiles derived from the standard THINGS moment-zero maps in Figure 2. There is still a difference between the column densities derived from the moment-zero maps and from the stacking method despite the deeper cleaning of our data cubes. This small difference is due to the stacking of residual uncleaned emission in the data cubes, leading to somewhat higher fluxes. This effect can be corrected for in the moment maps, but less easily so for stacked profiles. We refer to Ianjamasimanana et al. (2017) for an extensive discussion. The small offset, however, does not affect the conclusions of this paper. The moment-zero values can only be reliably determined above 3 times the local rms noise. Note that the rms noise in a moment zero map is not the same as the rms noise in a data cube channel map since a variable number of channels, N , contribute to any given pixel in the moment map. We therefore calculate the rms noise in the moment maps as the rms noise in one channel map multiplied by the square root of the number of the contributing channels. This assumes channels are independent, which is a valid assumption as the THINGS data are Hanning-smoothed (see Walter et al. 2008). We indicate the (moment-zero) column density sensitivity corresponding to 3 times the rms noise in Figure 2. We also show in the same figure the 3 times rms noise col-

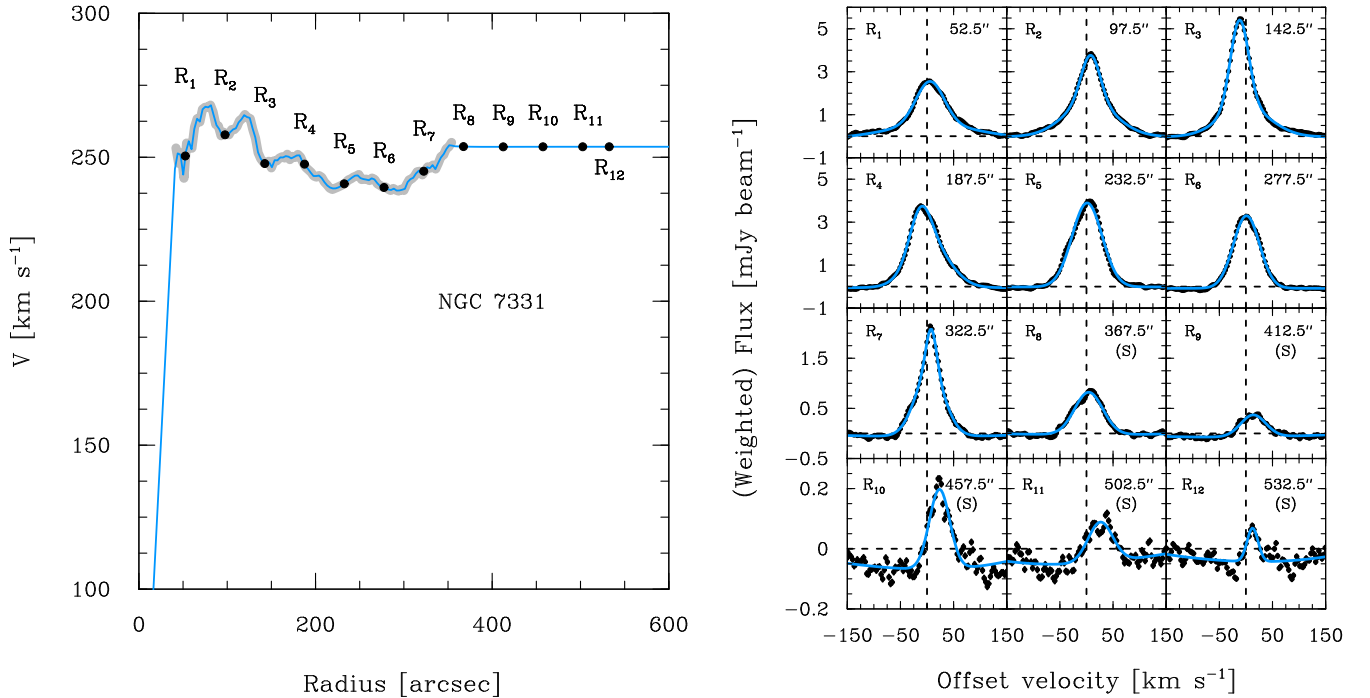


Figure 1. Left: the observed rotation curve of NGC 7331 (thick gray line, [de Blok et al. 2008](#)) and our interpolation and extrapolation of the rotation curve (blue solid line). Right: Azimuthally averaged stacked profiles of NGC 7331 (black circle symbols). The solid blue lines are the fit to the data. The vertical and horizontal dashed lines indicate the flux and offset velocity with respect to the model velocity field to guide the eyes. The (S) letters in some panels represent the ‘stacked radii’, i.e., the spectra at a radius larger than the extent traced directly by the THINGS moment zero map.

umn density sensitivity of the azimuthally stacked profiles. On average, the stacking method offers an order of magnitude sensitivity improvement compared to the traditional moment-zero analysis. Close inspection of Figure 2 shows that the stacked profiles do not always reach the $S/N = 3$ limit. In these cases we are limited by the presence of low-level artefacts in the data (mostly due to deconvolution residuals) that prevent us from reaching lower limits. Nevertheless, the fact that with the current data set stacking already yields limits much lower than traditional moment-zero limits, clearly shows the promise of the method.

The most surprising finding from Figure 2 is that most galaxies show no evidence of a break. The profiles are mostly flat in the inner disk and then decline smoothly down to the sensitivity limit of our (stacked) data. Our assumption of a flat rotation curve cannot be the reason for this absence of an HI break. Any incorrect estimates of the rotation curves would result in stacked profiles that are systematically lower in amplitude but broader in width and this would not remove the signature of a break. A major velocity offset between real and assumed velocities would result in non-detections, which would mimic an artificially strong break in the profiles.

A possible cause of the absence of a break is that the HI surface density distribution is azimuthally asymmetric. Our sample galaxies exhibit this asymmetry. These

include, among others, NGC 7331, NGC 3198, NGC 2903, NGC 3621. We also note that the break in M33 observed by [Corbelli et al. \(1989\)](#) is based on a single radial slice along the major axis of the galaxy. In addition, the break in NGC 3198 observed by [van Gorkom \(1993\)](#) (see also [Heald et al. 2016](#); [Kam et al. 2017](#)) is seen in only one side of the galaxy. Thus the stacking method may smooth out any potential break as we are averaging over the full azimuthal angle. To explore this possibility, we also divide the galaxies into 30 degree wide ‘‘pie-wedge-shaped’’ sectors and do the stacking inside annular sectors instead of the full azimuthal annuli. The results are shown in Figure B1 of the Appendix. Although the radial profiles are steeper in some sectors than in others, the profiles are smooth without a clear break. We thus conclude that the absence of a break in the (full) azimuthally averaged profiles are not caused by the presence of an asymmetric HI distribution.

4.3. Exceptions

A close inspection of the individual galaxies reveals that there are a few exceptions to the conclusion that radial breaks are not present in this sample. These are discussed in the following. The radial profiles of NGC 4736 and NGC 3621 decline steeply around 10^{20} cm^{-2} and for NGC 4826 at $\sim 5 \times 10^{19} \text{ cm}^{-2}$. These three galaxies, however, have some structural peculiarities.

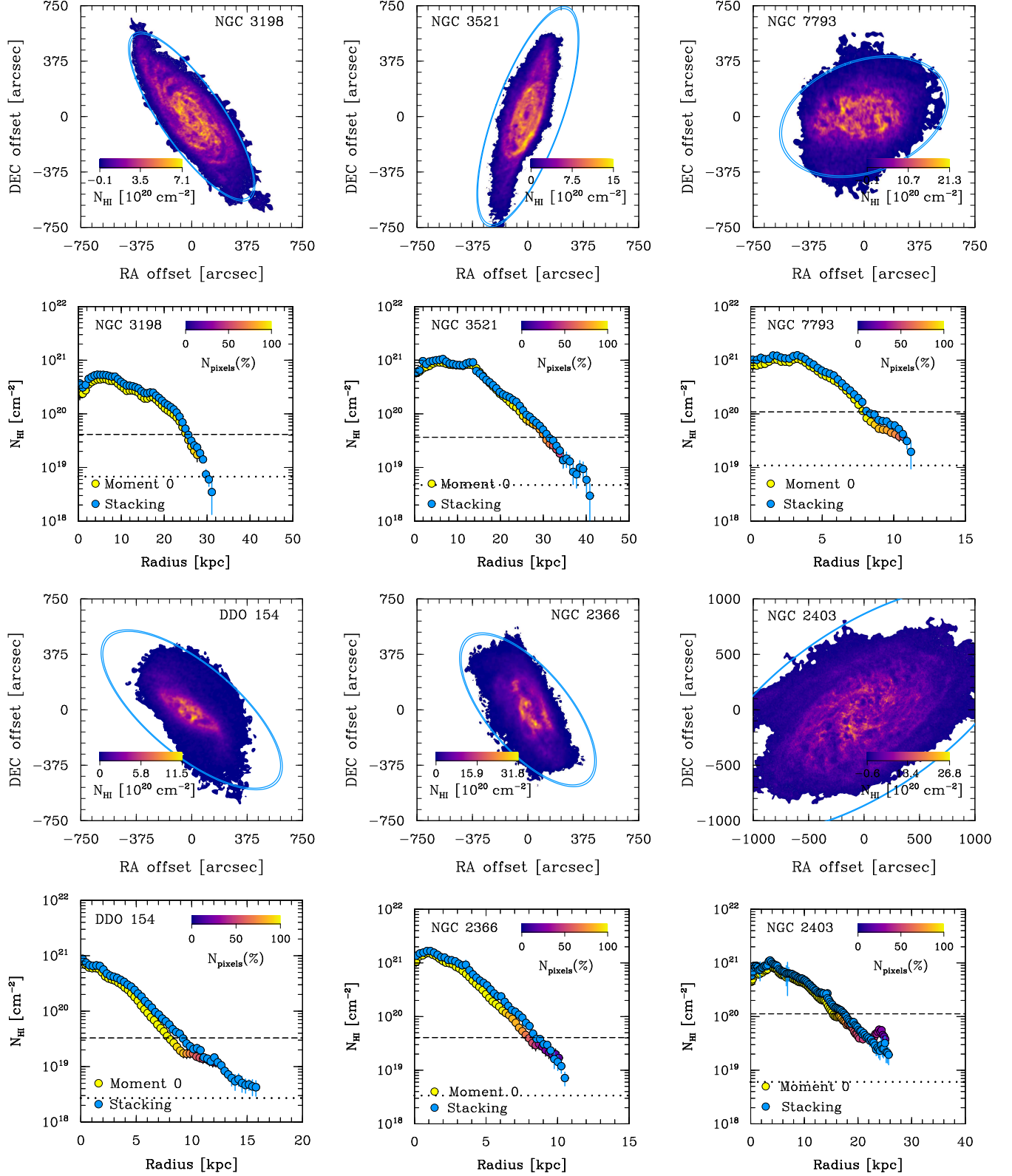


Figure 2. Odd rows: H I column density maps overlaid with blue ellipses showing the annuli used to derive the radial profiles (only the outermost annulus is shown). Even rows: the radial H I column density profiles of our sample galaxies. The blue solid circle symbols represent the radial profiles derived from our stacking method. The color-coded (the color represents the number of pixels inside each annulus in %) solid circle symbols show the azimuthally averaged radial profiles derived from the THINGS moment zero maps. The horizontal dashed lines correspond to the sensitivity of the THINGS moment zero maps (3 times the rms noise). The dotted lines represent the sensitivity of the azimuthally stacked profiles corresponding to 3 times the rms noise.

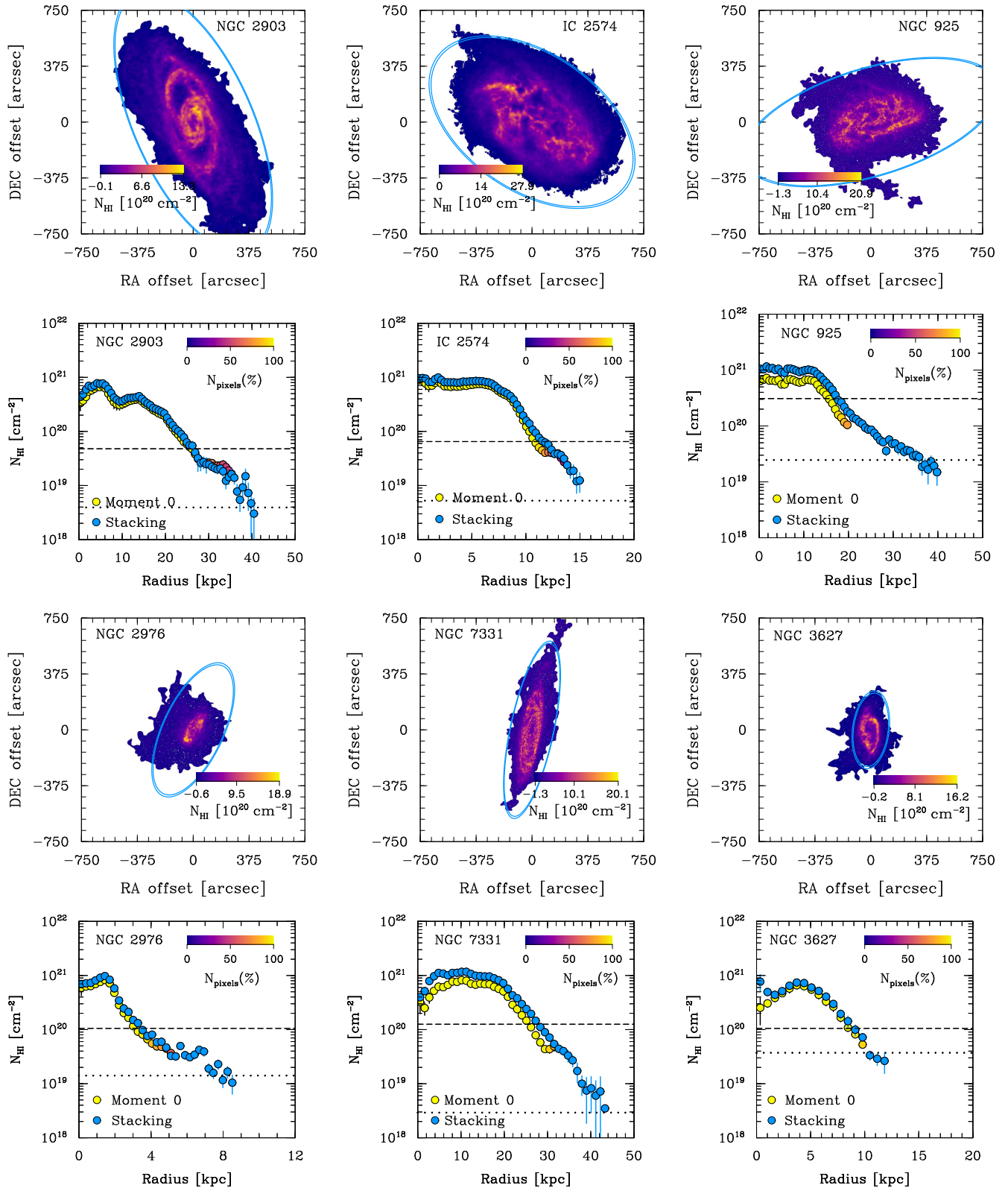


Figure 2. Continued.

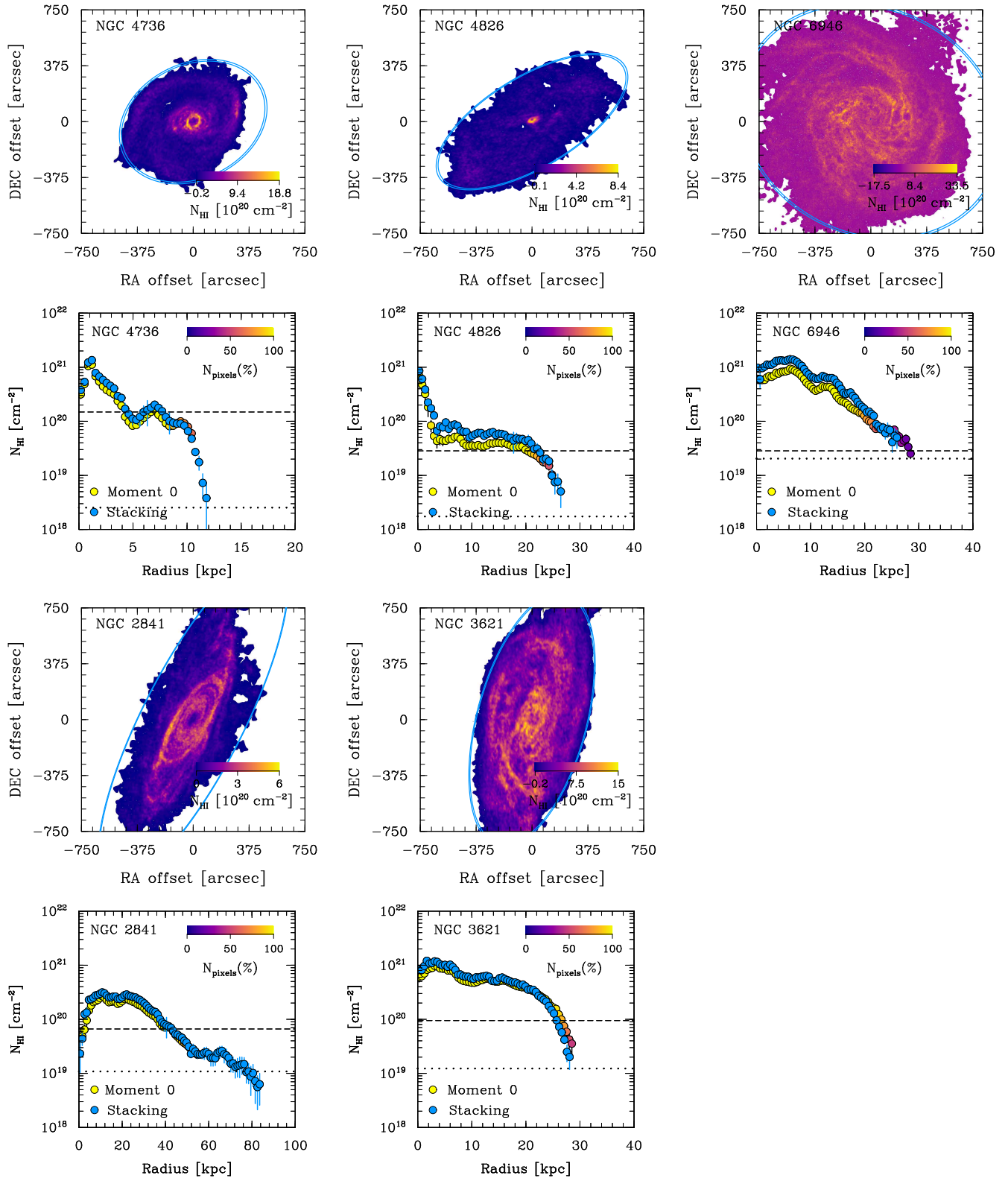


Figure 2. Continued.

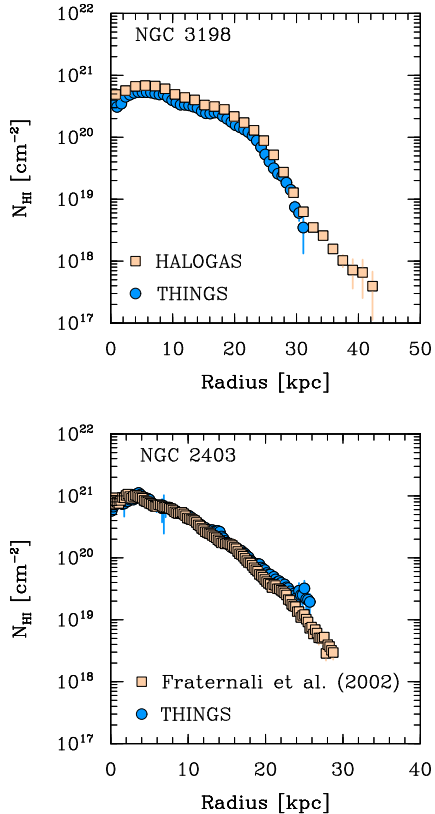


Figure 3. Radial H I column density profiles of NGC 3198 and NGC 2403, showing both the results based on the THINGS and HALOGAS data. We find good agreement between the two independent methods to analyze the data.

NGC 4736 has a ring-like H I morphology which manifests itself as bumps in the H I column density profiles shown in Figure 2. Earlier lower resolution H I observations by Bosma et al. (1977) also revealed this pattern. The authors classified the galaxies as consisting of 5 different zones in which a faint outer ring surrounds the main body of the galaxy. The H I edge around 7 kpc corresponds to the transition from the main disk of the galaxy and the faint outer rings identified by Bosma et al. (1977). The origin of the ring is not clear but could be related to a past accretion event. Due to the high column-density at which it occurs ($\sim 10^{20} \text{ cm}^{-2}$), it is unlikely that the H I break is related to the breaks driven by ionization. NGC 3621, on the other hand, has an extended H I distribution. The integrated H I intensity map shows a tail or stream of gas extending along the major axis, which could be the result of past interactions or signatures of gas accretion. The break around 10^{20} cm^{-2} for this galaxy therefore corresponds to the transition between the main disk of NGC 3621 and the stream or tail (See also Figure B1). The profile of NGC 4826 declines steeply around $5 \times 10^{19} \text{ cm}^{-2}$. However, it is unlikely that we are tracing effects due to ionization by extragalactic photons. Kinematical studies by Braun

et al. (1994) and by Rix et al. (1995) revealed that the inner disk is counter-rotating with respect to the outer disk. As reported by Rix et al. (1995), this counter-rotation may indicate that the outer disk of NGC 4826 has been built from the merging of gas rich dwarf galaxies or from the infall of H I gas with a retrograde orbit. Regardless of the exact cause, it is conceivable that we are tracing the relics of a merging event or episodic gas infall rather than the effects of photoionization. In the discussion that follows we do not include the three galaxies discussed in this section.

4.4. Comparison with HALOGAS

For two galaxies we have both THINGS and HALOGAS data available. This provides us with the opportunity to check for possible systematics. In Figure 3, we overplot the azimuthally stacked THINGS and HALOGAS H I column density profiles for NGC 2403 and NGC 3198. In both cases, we find excellent agreement in the measurements (where they overlap). Also, neither galaxies column density show any indication for a break in H I, but feature rather smooth profiles.

4.5. Identification of any possible breaks and comparison with models

To better identify possible breaks in the azimuthally stacked profiles, we measure the change in slope of the profiles by calculating their first logarithmic derivatives. We also use the first logarithmic derivatives to gauge whether any break seen in the data resembles that of the photoionization models of Maloney (1993) and Dove & Shull (1994). The derivative will be zero for a constant profile, negative if it is decreasing and positive if the profile is increasing. As illustrated in Figure 4, the change in slope is close to zero for many galaxies and does not resemble that of the photoionization models. Note that the models by Maloney (1993) and by Dove & Shull (1994) only show $N_{\text{HI}}(R)$ for $R \geq 20$ kpc. Purely for illustrative purposes, we thus extrapolated the models to $R = 0$ kpc. The clear difference between the observed and model profiles shows that with our present data, we do not find convincing evidence that would suggest the presence of a break caused by photoionization in our column density profiles.

To quantify the amount of change in slope, we fit the profiles using Sérsic profiles (Sérsic 1968) with different slope indexes, n . We here use the formalism introduced by Portas (2010) who, for $n < 1$, defines the Sérsic profile in terms of a break radius, R_b , instead of the half-light radius that is mostly used in the literature. Thus, following Portas (2010), we define the Sérsic profile as:

$$I(R) = I(0) \exp \left\{ -(1-n) \left(\frac{R}{R_b} \right)^{1/n} \right\}, \quad (3)$$

where $I(0)$ is the central intensity. We vary the slope indexes, n , but fix $I(0)$ and R_b and derive the first logarithmic derivatives of the resulting profiles. As seen in Figure 5, a Sersic index of 0.46 roughly corresponds to a derivative value of $-0.2 \text{ dex cm}^{-2} \text{ kpc}^{-1}$. We create a second set of synthetic profiles consisting of a straight line without a break and straight lines that break at a fixed radius, R_b , with varying slopes. We illustrate those results in Figure 5. Here an order of magnitude decrease within 3 kpc (corresponding to $f=10$ in the Figure) corresponds to a derivative value change of $-0.3 \text{ dex cm}^{-2} \text{ kpc}^{-1}$. Note that the values of the derivatives of the real data are typically $\gtrsim -0.2 \text{ dex cm}^{-2} \text{ kpc}^{-1}$. The photoionization models by Maloney (1993) and Dove & Shull (1994), on the other hand, have derivative values $\lesssim -0.3 \text{ dex cm}^{-2} \text{ kpc}^{-1}$. We conclude that, down to our sensitivity limit, a radial column density break is not a common feature of disk galaxies. More high sensitivity HI observations are needed to investigate the HI distribution at even lower column density values.

4.6. NGC 3198: Comparison with van Gorkom (1993)

NGC 3198 is a galaxy for which we do not find a global break in neither the THINGS nor the HALOGAS data. However, van Gorkom (1993) reported a break toward the approaching side of this galaxy. She showed that the column density of NGC 3198 decreased by an order of magnitude within a synthesized beam of 2.7 kpc. When we redo the analysis for the approaching side of NGC 3198, we did not find a noticeable break as reported by van Gorkom (1993). This prompted us to redo the analysis for the approaching and receding sides of all galaxies. To allow a better comparison of our data with that of van Gorkom (1993), we divide the radial profiles of the approaching and receding sides of the galaxies in 2.7 kpc bins, thus using the same definition for the slope as van Gorkom (1993). We then calculate the slopes of the outer $N_{\text{HI}}(R) \leq 10^{20} \text{ cm}^{-2}$ as $N_{\text{HI}}(R)/N_{\text{HI}}(R + 2.7)$ (see Figure 6). From this analysis, we do not find evi-

dence that an HI break associated with ionization is a common feature in galaxies.

5. SUMMARY AND CONCLUSION

We studied the radial HI column density profiles of 17 nearby galaxies. We used data from the THINGS and, for two galaxies, the HALOGAS survey. To push the sensitivity limit of our data to deeper levels and trace the HI distribution to previously unexplored radii, we stacked individual profiles azimuthally using a stacking technique. Model velocity fields derived from a simple (flat) extrapolation of the rotation curves were used to stack individual profiles at large radii. In general the radial column density profiles are flat in the inner disk and then smoothly decline down to the sensitivity limit of the data. Thus, our present data do not confirm the prediction of photoionization models that an HI break at a column density of $\sim 5 \times 10^{19} \text{ cm}^{-2}$ is a common feature of HI disks. The absence of an HI break may indicate that ionization by extragalactic photons is not the limiting factor of the extent of the HI disk. Thus, the outskirts of the HI disk may instead correspond to the transition to a low column density gas accreted from the cosmic web at later evolutionary stages of disk formation. However, in order to map the morphology and kinematics of the low column density outskirts, we require the next generation of radio telescopes (e.g., MeerKAT, de Blok 2011). Until then we can only start to trace the average properties at the outermost radii, as done in this paper.

The authors thank the anonymous referee for excellent comments that helped improve the presentation of this paper. R.I. acknowledges funding from the Alexander von Humboldt foundation through the Georg Forster Research Fellowship programme. EB acknowledges support from the UK Science and Technology Facilities Council [grant number ST/M001008/1]. We thank the HALOGAS team for providing us with the NGC 3198 and NGC 2403 data.

APPENDIX

A. AZIMUTHALLY STACKED SPECTRA

In this Section, we show the model rotation curves used to derive the radial surface density profiles of our sample galaxies (see Figure A1). We also show examples of the azimuthally averaged stacked spectra at different radius (see Section 3 for details).

B. RADIAL COLUMN DENSITY PROFILES AS A FUNCTION OF AZIMUTHAL POSITIONS

Here we present the radial profiles derived inside the annular sectors described in Section 4. In summary, the galaxies are divided into concentric rings with widths close to the synthesized beam of the observations. All rings are then split into 30 degree wide sectors, resulting in annular sectors as shown in Figure B1 (only the outer-most annular sectors are shown). The stacking of individual profiles at a given radius are done inside the annular sectors to obtain the radial column density profiles shown in Figure B1.

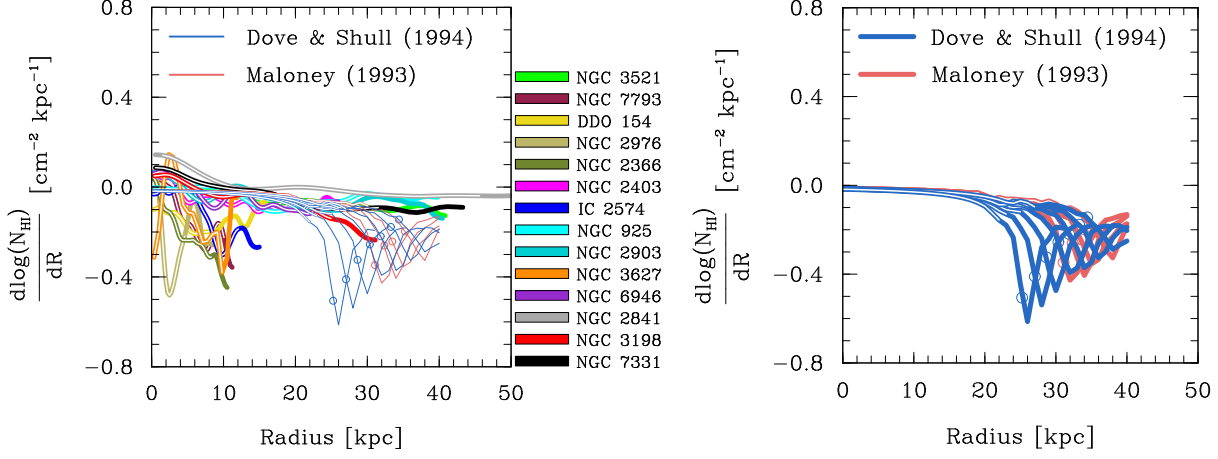


Figure 4. Left: first logarithmic derivatives of the radial column density profiles of our sample galaxies (thick solid lines) overplotted on the photoionization models (thin solid lines) by Maloney (1993) and by Dove & Shull (1994). Right: The photoionization models shown as thin lines in the left panel are re-plotted for better visualization. The open lines indicate column densities above $5 \times 10^{19} \text{ cm}^{-2}$. The open circle symbols indicate at which radius the column densities drop below 10^{19} cm^{-2} .

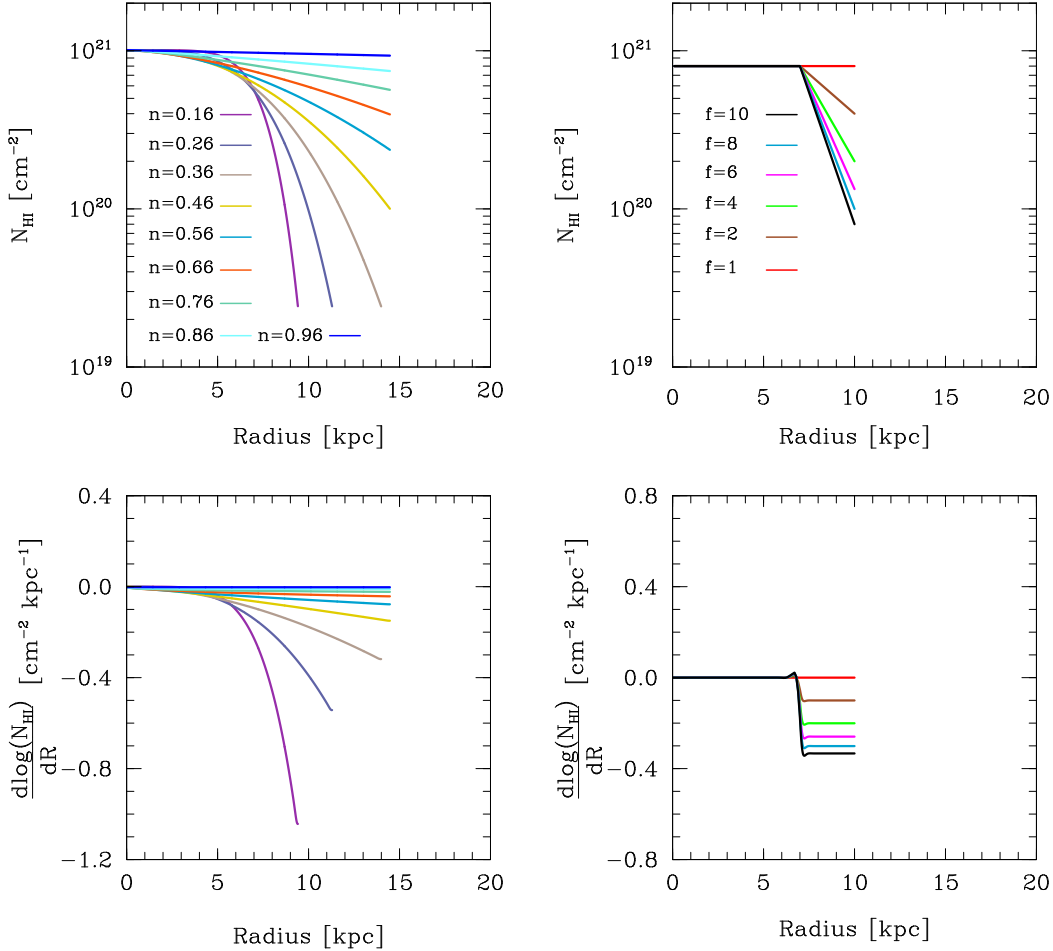


Figure 5. Solid lines: synthetic column density profiles (top panels) and their respective first logarithmic derivatives (bottom panels).

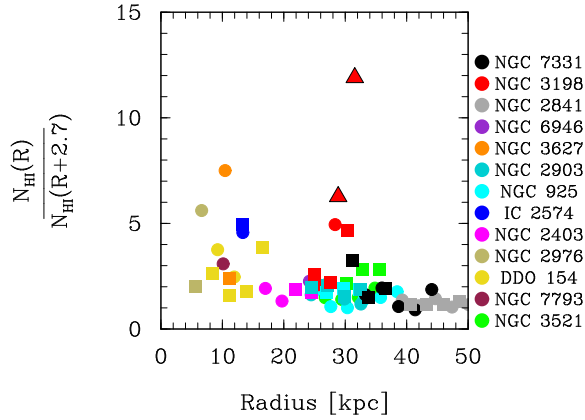


Figure 6. Slopes of the approaching and receding radial column density profiles within 2.7 kpc (see text for motivation). Only the outer-radii corresponding to $N_{\text{HI}}(R) \leq 10^{20} \text{ cm}^{-2}$ are shown. Circle symbols: approaching sides; square symbols: receding sides. Triangle symbols: slopes derived from the [van Gorkom \(1993\)](#) data (approaching side).

REFERENCES

- Bergeron, J., & Gunn, J. E. 1977, *ApJ*, 217, 892
- Bosma, A., van der Hulst, J. M., & Sullivan, W. T., III 1977, *A&A*, 57, 373
- Bosma, A. 1981, *AJ*, 86, 1825
- Braun, R., Walterbos, R. A. M., Kennicutt, R. C., Jr., & Tacconi, L. J. 1994, *ApJ*, 420, 558
- Briggs, D. S. 1995, High Fidelity Deconvolution of Moderately Resolved Sources, PhD Thesis, New Mexico Institute of Mining and Technology
- Broeils, A. H., & van Woerden, H. 1994, *A&AS*, 107
- Carignan, C., Frank, B. S., Hess, K. M., et al. 2013, *AJ*, 146, 48
- Corbelli, E., Schneider, S. E., & Salpeter, E. E. 1989, *AJ*, 97, 390
- Corbelli, E., & Salpeter, E. E. 1993, *AJ*, 419, 104
- de Blok, W. J. G., Walter, F., Brinks, E., et al. 2008, *AJ*, 136, 2648
- de Blok, W. J. G. 2011, *Tracing the Ancestry of Galaxies*, 277, 96
- Dove, J. B., & Shull, J. M. 1994, *ApJ*, 423, 196
- Fraternali, F., van Moorsel, G., Sancisi, R., et al. 2002, *AJ*, 123, 3124
- Fumagalli, M., Haardt, F., Theuns, T., et al. 2017, *MNRAS*, 467, 4802
- Heald, G., Józsa, G., Serra, P., et al. 2011, *A&A*, 526, 118
- Heald, G., de Blok, W. J. G., Lucero, D., et al. 2016, *MNRAS*, 462, 1238
- Ianjamasimanana, R., de Blok, W. J. G., Walter, F., & Heald, G. H. 2012, *AJ*, 144, 96
- Ianjamasimanana, R., de Blok, W. J. G., & Heald, G. H. 2017, *AJ*, 153, 213
- Irwin, J. 1995, *PASP*, 107, 715
- Irwin, J. A., Hoffman, G. L., Spekkens, K., et al. 2009, *ApJ*, 692, 1447
- Kam, S. Z., Carignan, C., Chemin, L., et al. 2017, *AJ*, 154, 41
- Maloney, P. 1993, *ApJ*, 414, 41
- Oh, S.-H., de Blok, W. J. G., Walter, F., Brinks, E., & Kennicutt, R. C., Jr. 2008, *AJ*, 136, 2761-2781
- Oosterloo, T., Fraternali, F., & Sancisi, R. 2007, *AJ*, 134, 1019
- Portas, A. M. P., From giants to dwarfs : probing the edges of galaxies, 2010, Ph.D. Thesis
- Rix, H.-W. R., Kennicutt, R. C., Jr., Braun, R., & Walterbos, R. A. M. 1995, *ApJ*, 438, 155
- Sancisi, R. 1983, *Internal Kinematics and Dynamics of Galaxies*, 100, 55
- Sersic, J. L. 1968, *Cordoba, Argentina: Observatorio Astronomico*, 1968,
- Sunyaev, R. A. 1969, *Astrophys. Lett.*, 3, 33
- van Gorkom, J. H. 1993, In *The Environment and Evolution of Galaxies*, ed. J. M. Shull and H. A. Thronson, Jr. (Dordrecht, Kluwer), p. 345
- Walter, F., Brinks, E., de Blok, W. J. G., et al. 2008, *AJ*, 136, 2563

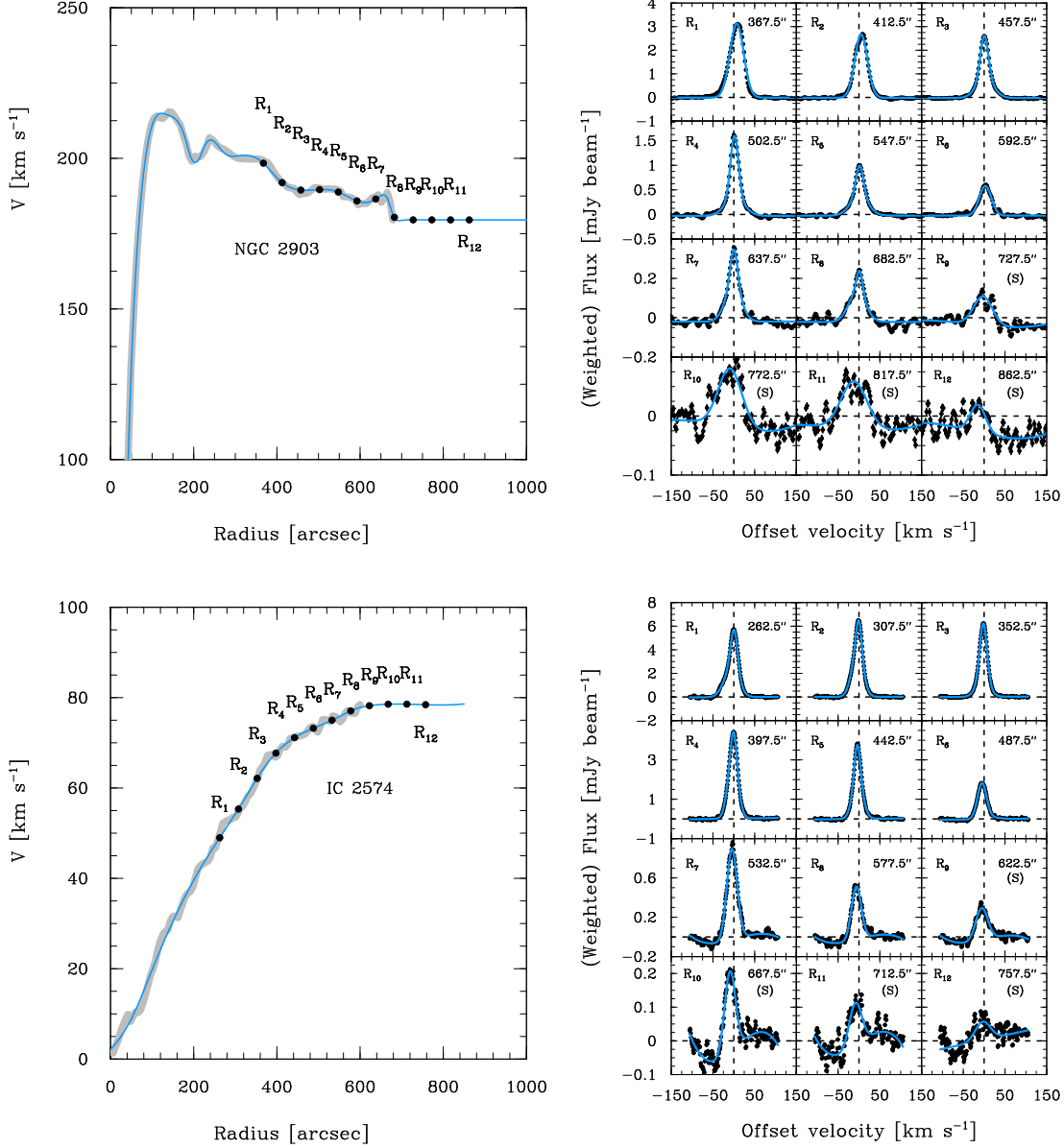


Figure A1. Left: the observed rotation curve by [de Blok et al. \(2008\)](#) (thick gray line) and our interpolation and extrapolation of the rotation curve (blue solid line). Right: Azimuthally averaged stacked profiles (black circle symbols). The solid blue lines are the fit to the data. The vertical and horizontal dashed lines indicate the flux and offset velocity with respect to the model velocity field to guide the eyes. The (S) letters in some panels represent the ‘stacked radii’, i.e., the spectra at a radius larger than the extent traced directly with the THINGS moment zero map.

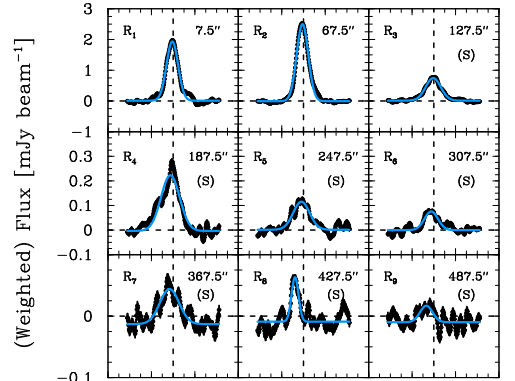
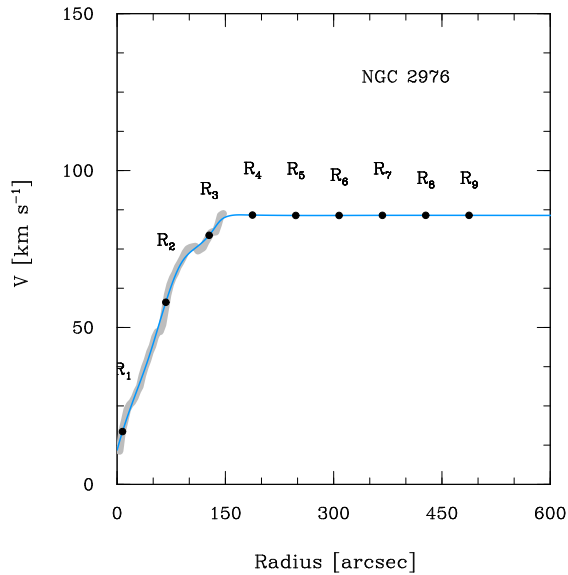
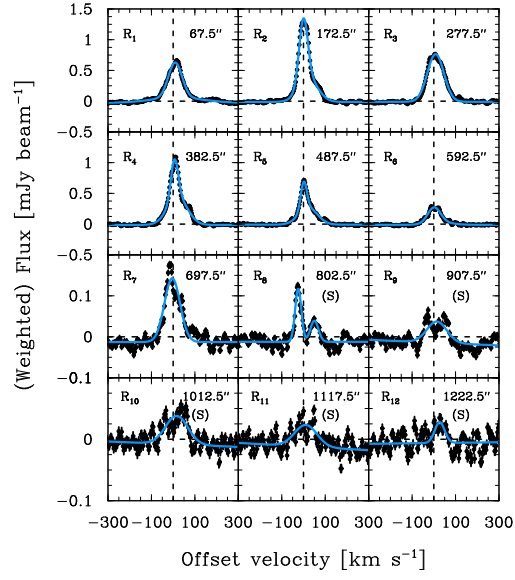
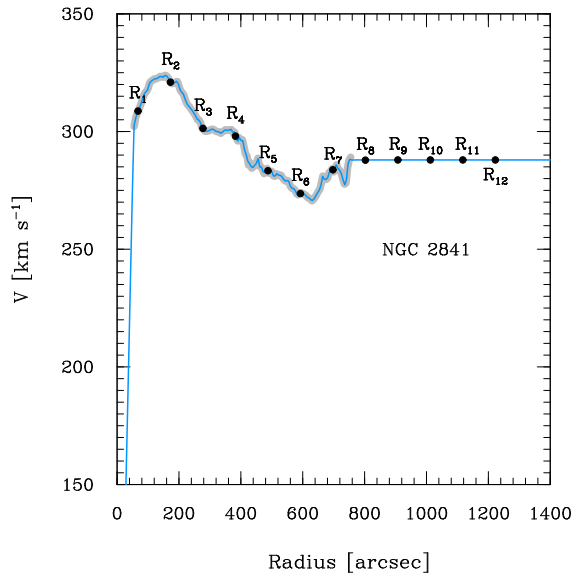
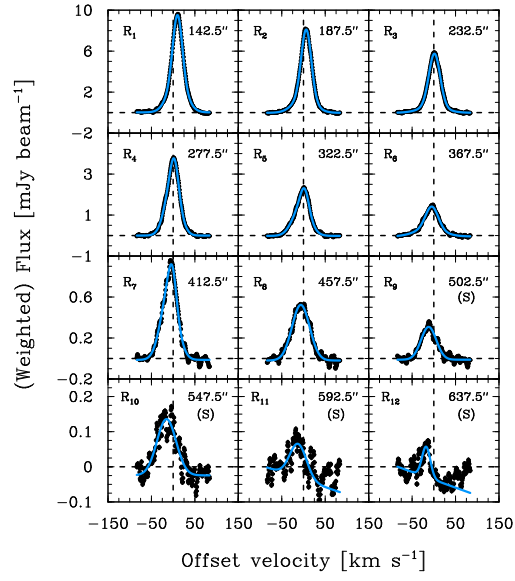
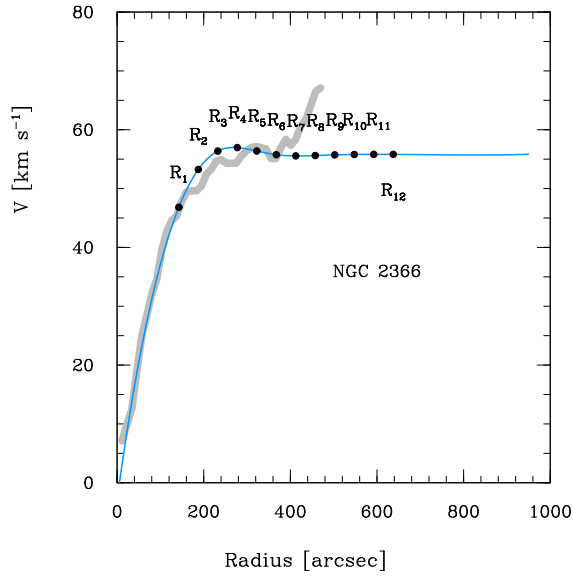


Figure A1. Continued.

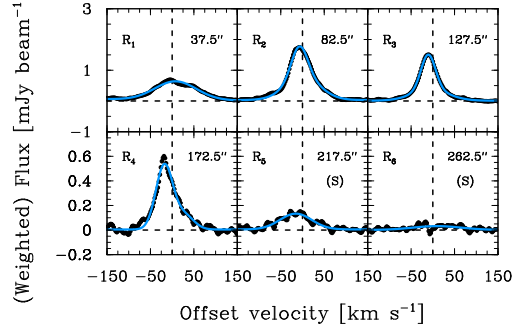
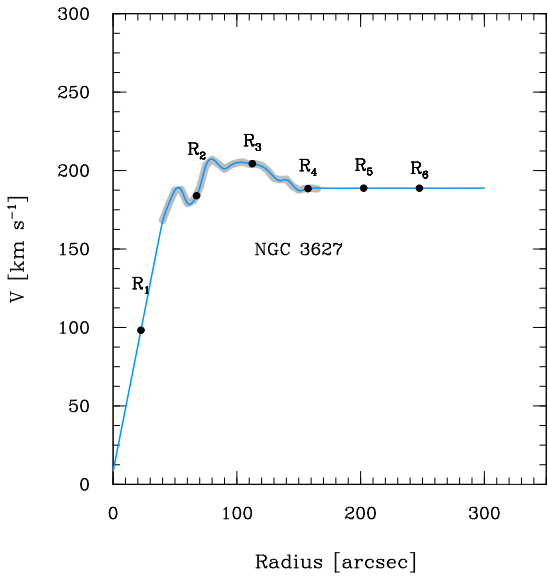
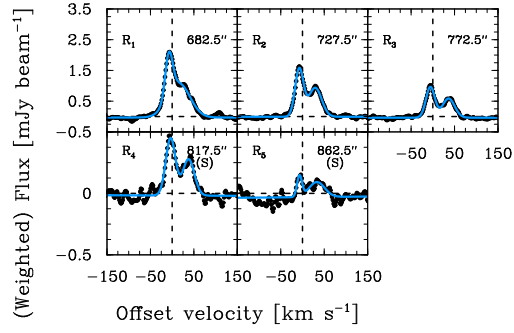
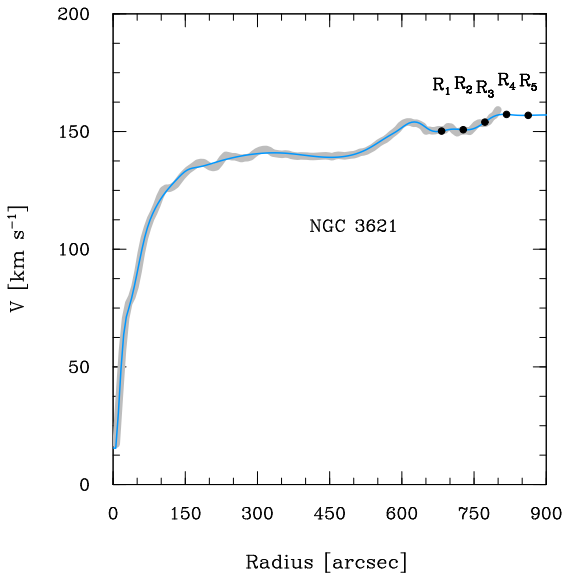
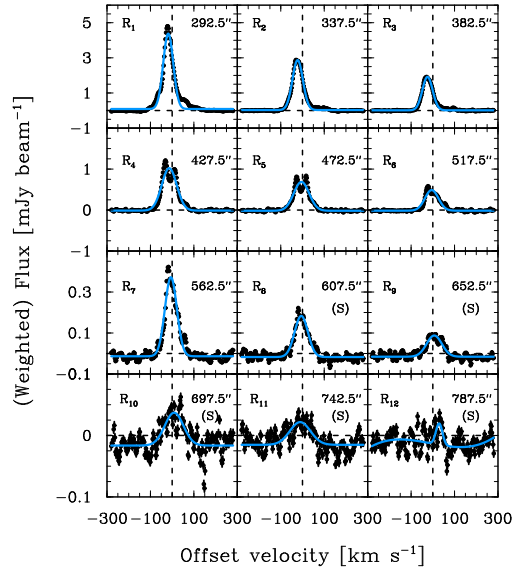
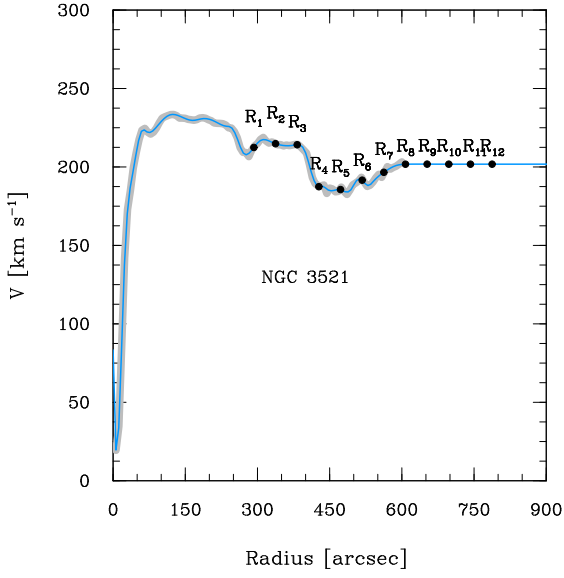


Figure A1. Continued.

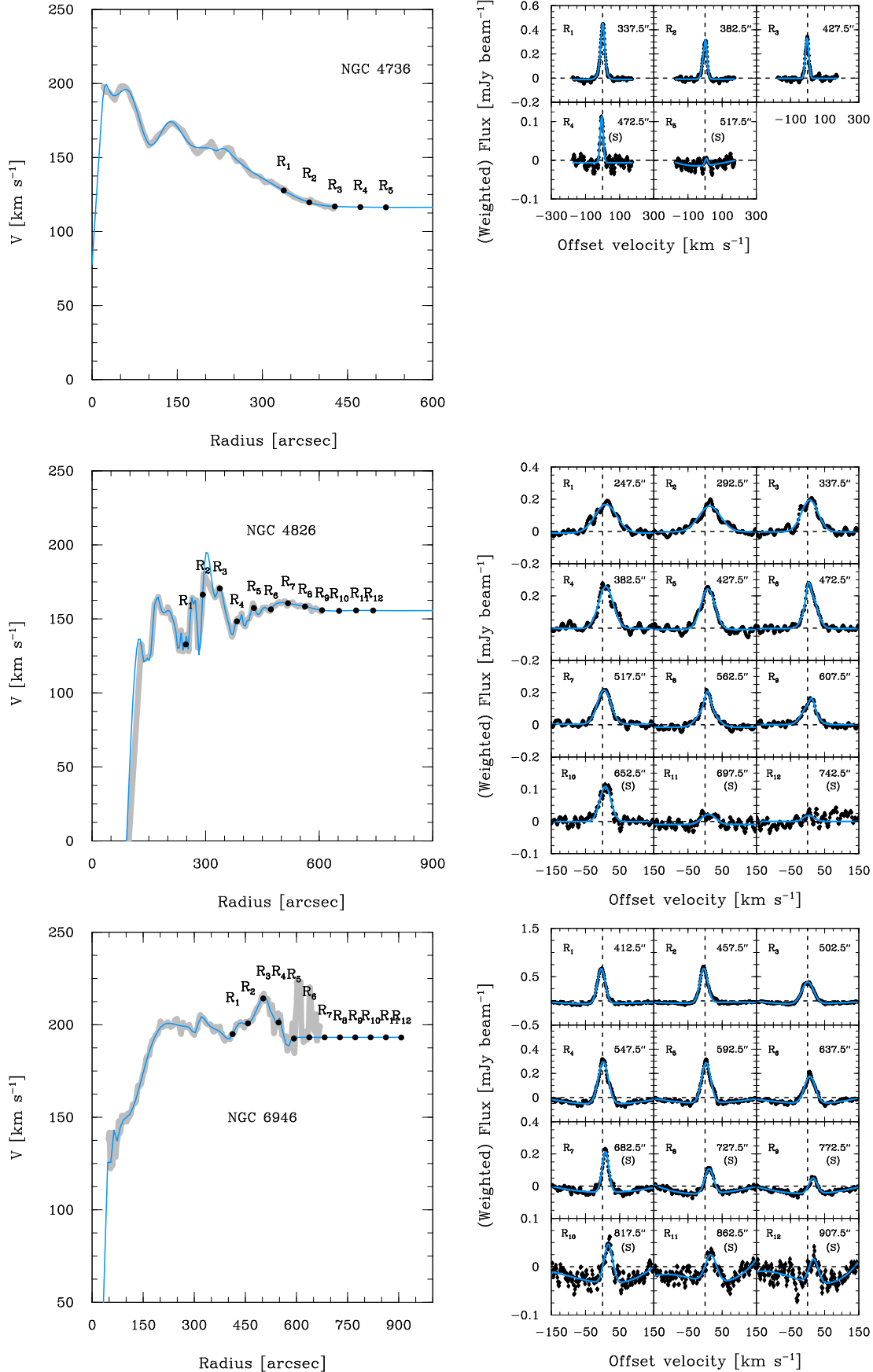


Figure A1. Continued.

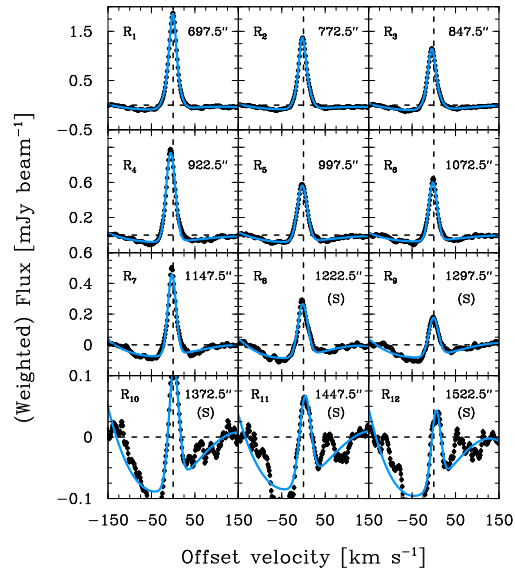
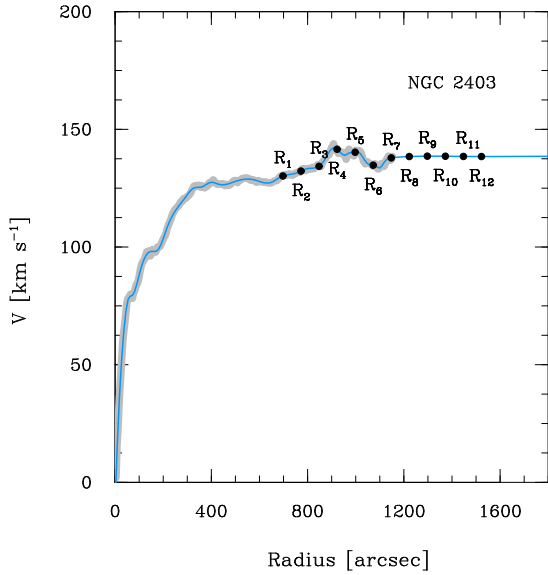
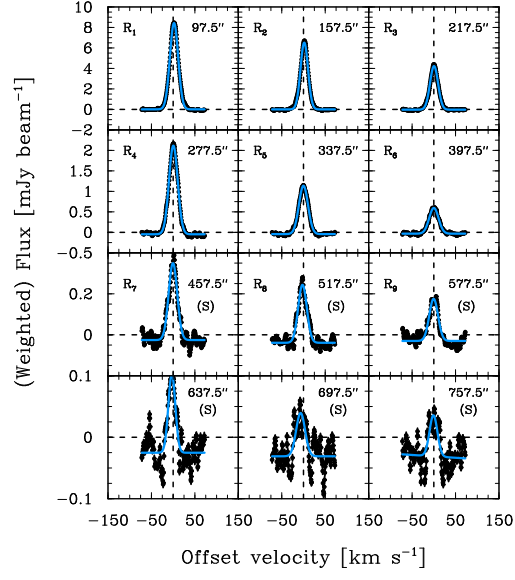
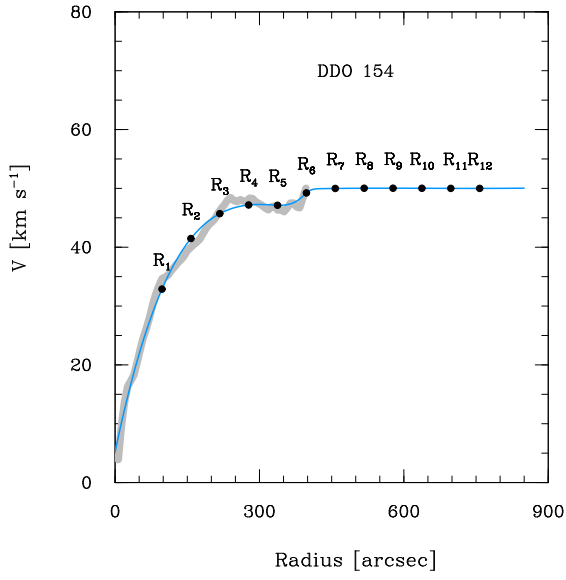
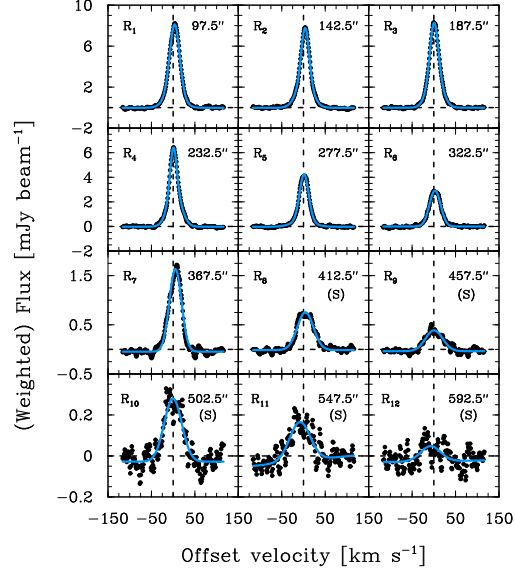
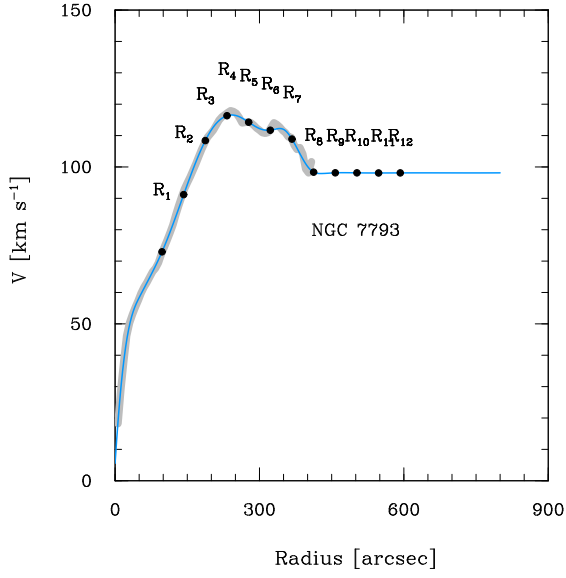


Figure A1. Continued.

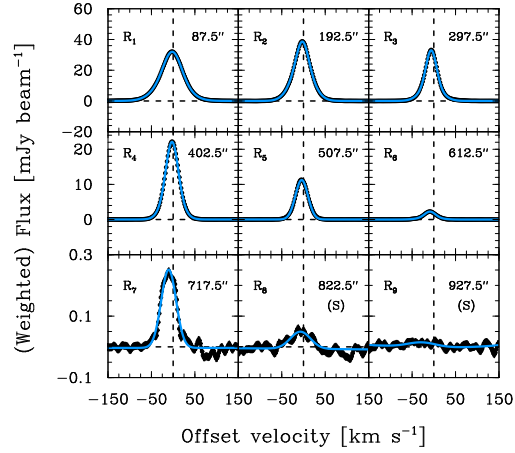
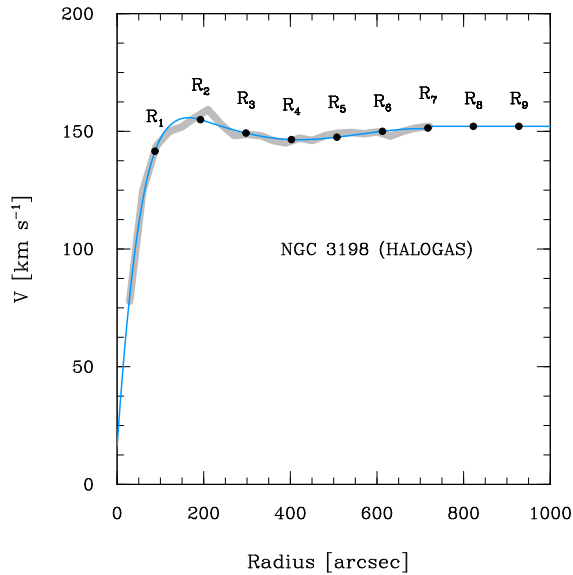
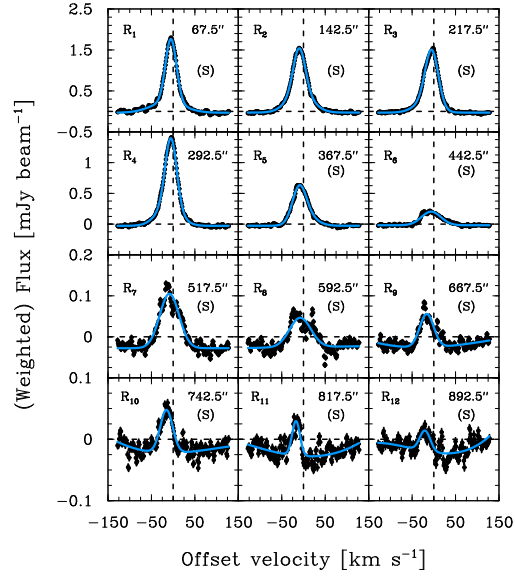
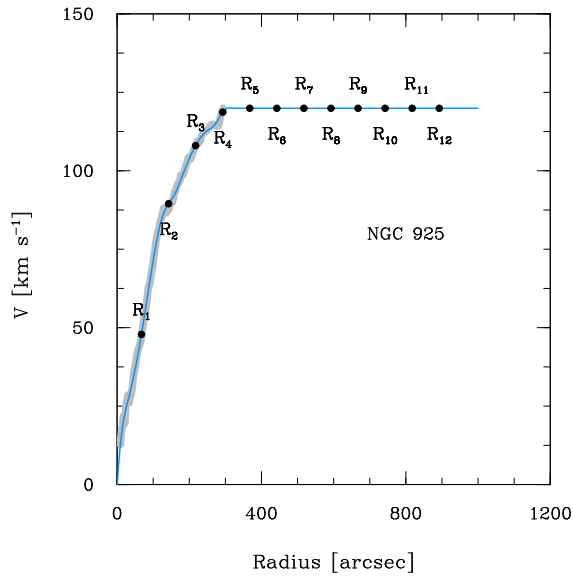
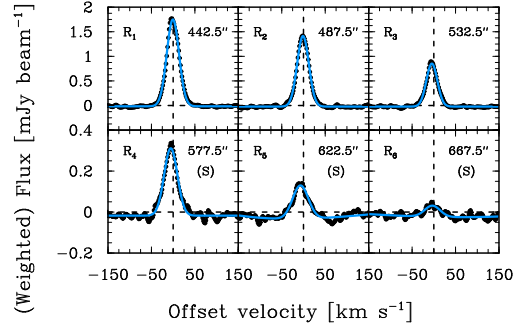
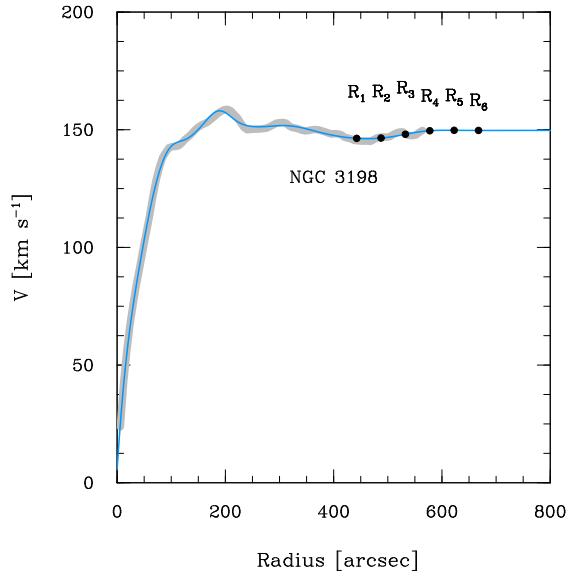


Figure A1. Continued.

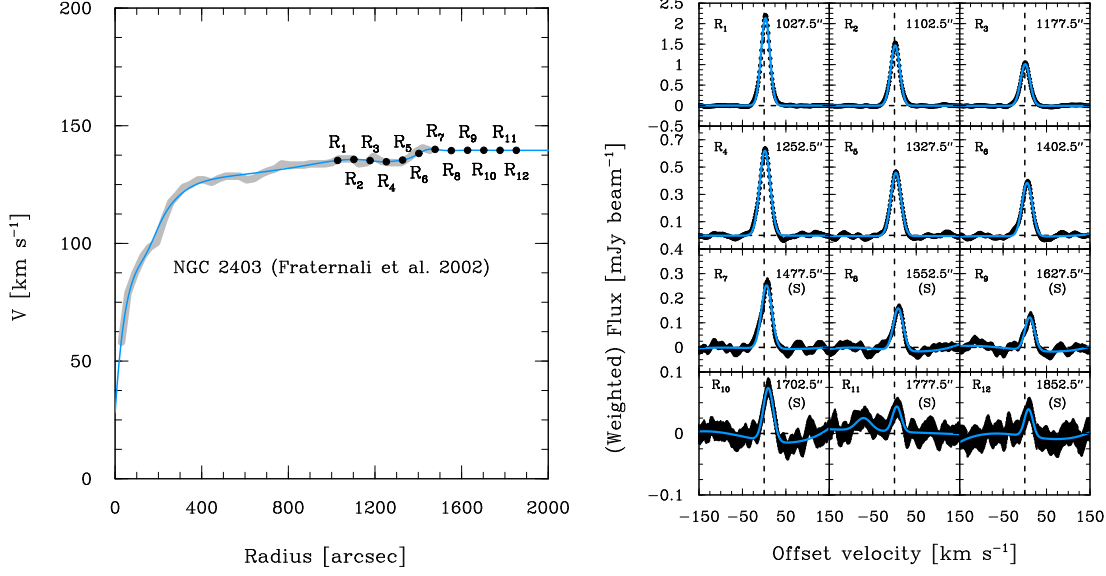


Figure A1. Continued.

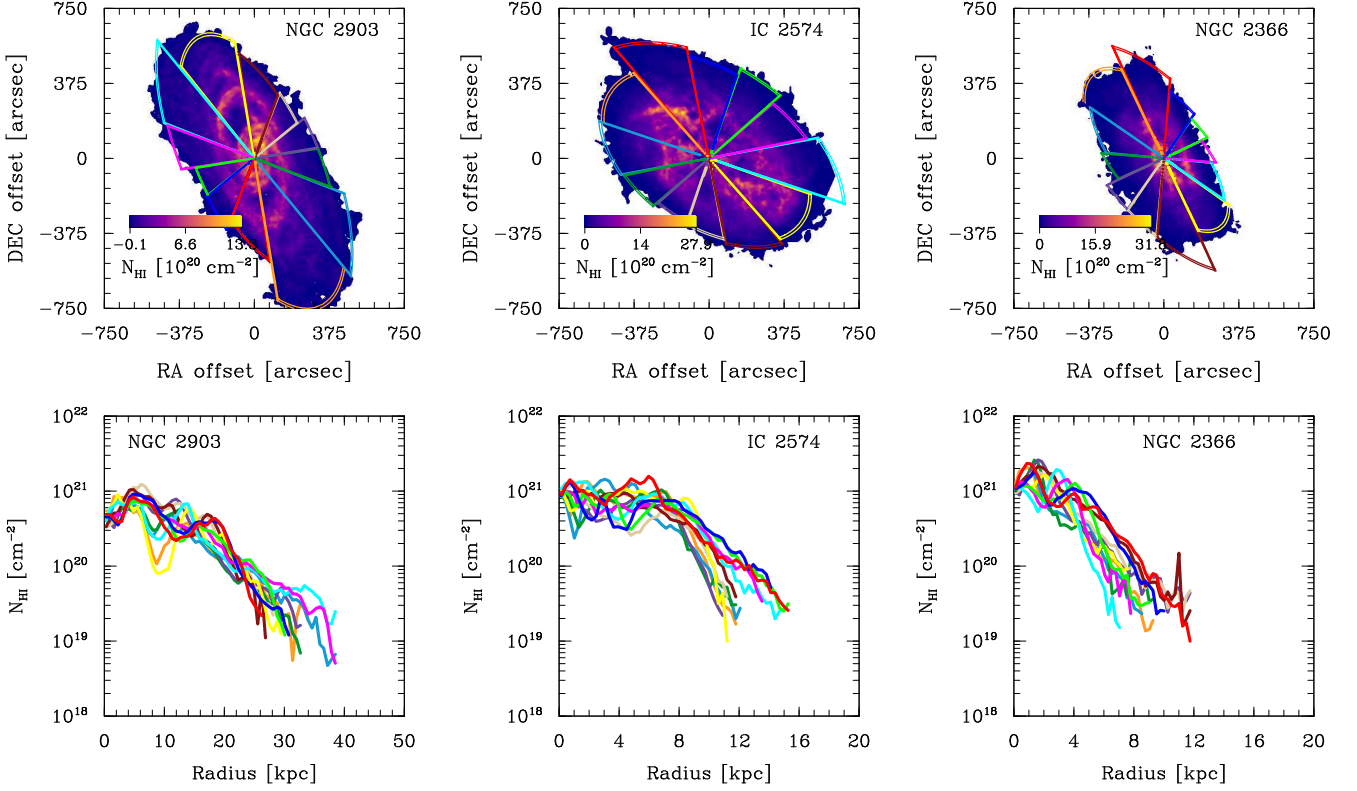


Figure B1. Odd rows: H I column density maps overlaid with the annular sectors inside which the radial profiles are derived (only the outermost annular sector is shown). Even rows: the radial H I column density profiles of the sample galaxies derived inside the different sectors. Different colors represent the different sectors used to derive the radial profiles.

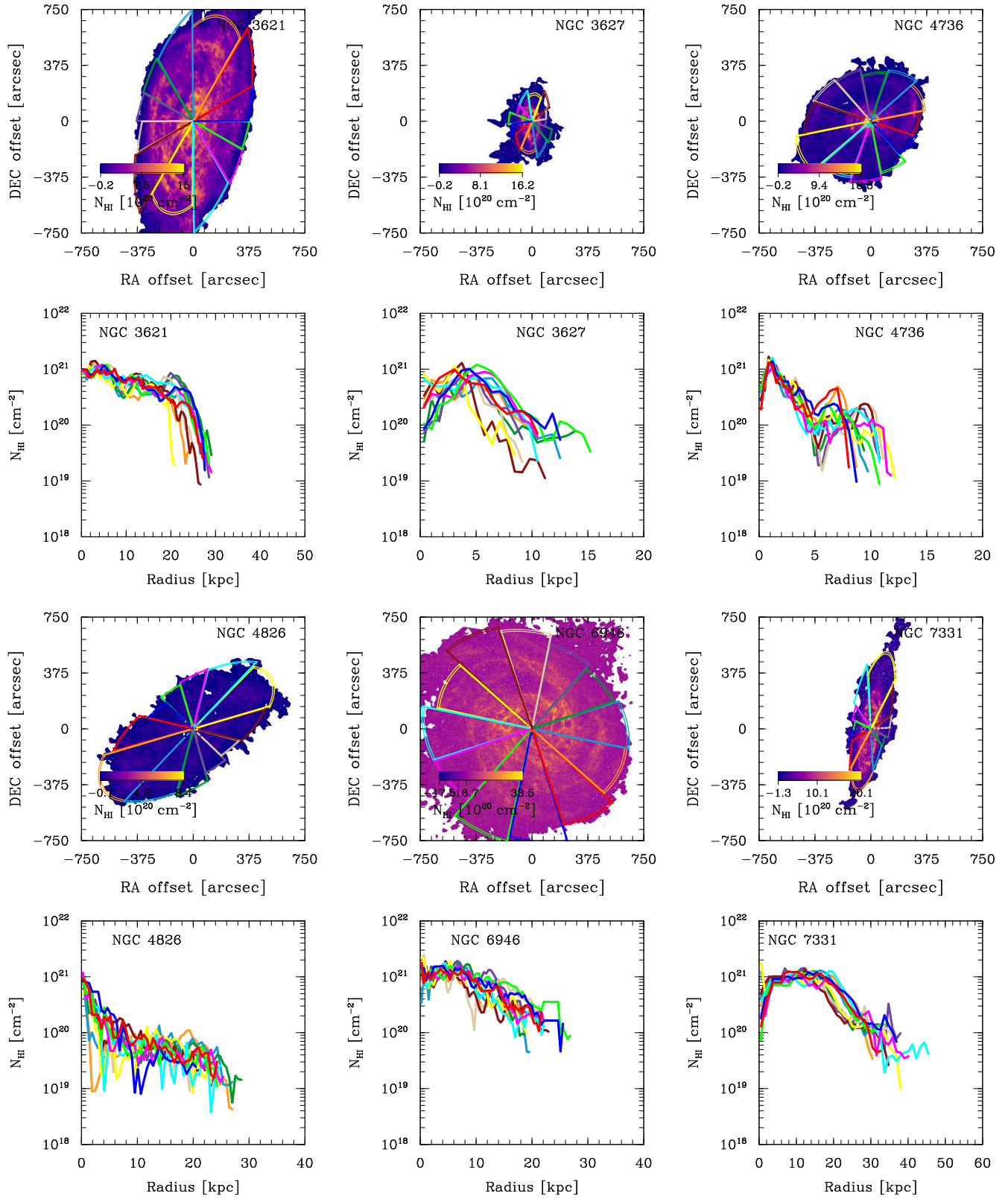


Figure B1. Continued.

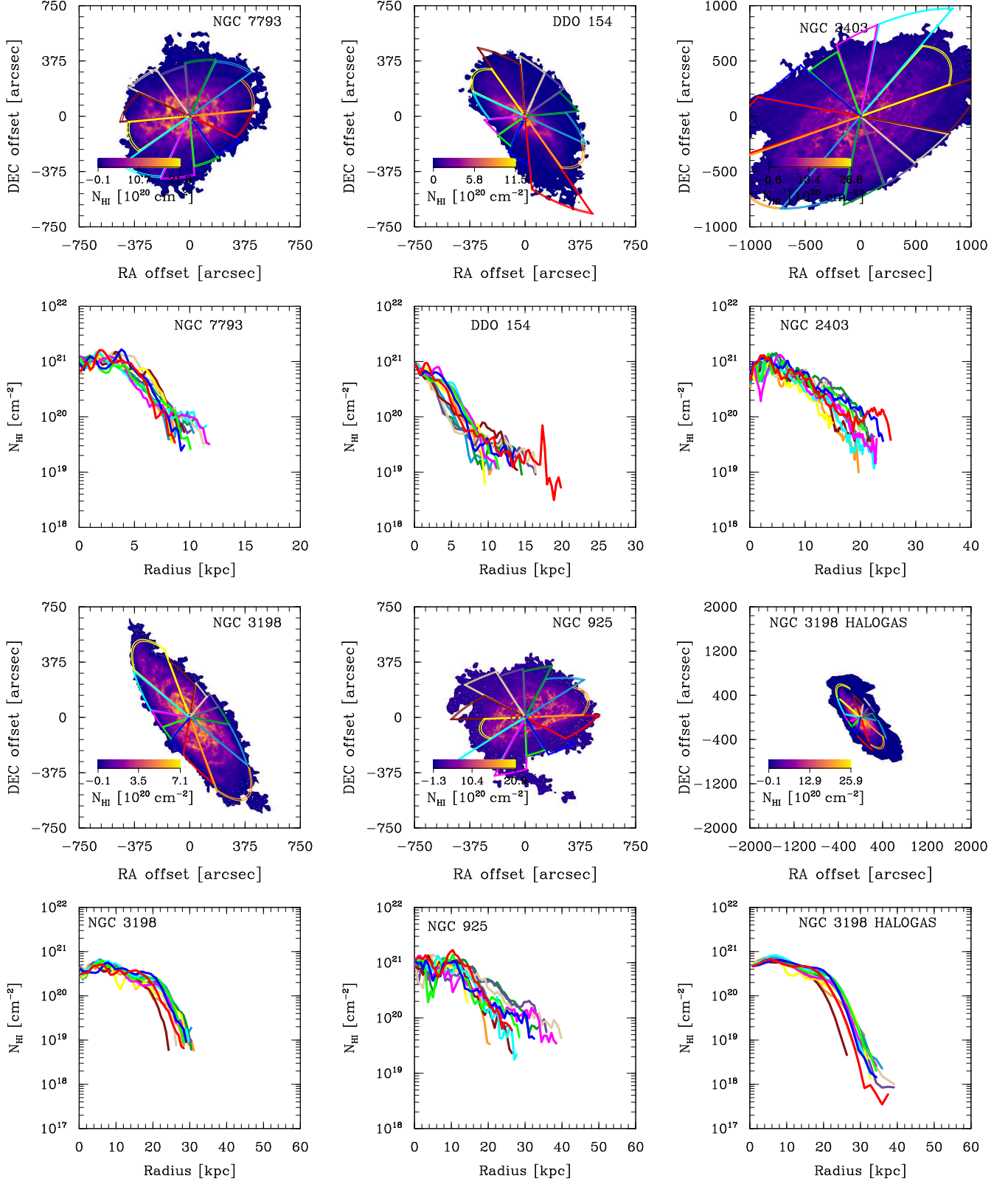


Figure B1. Continued.

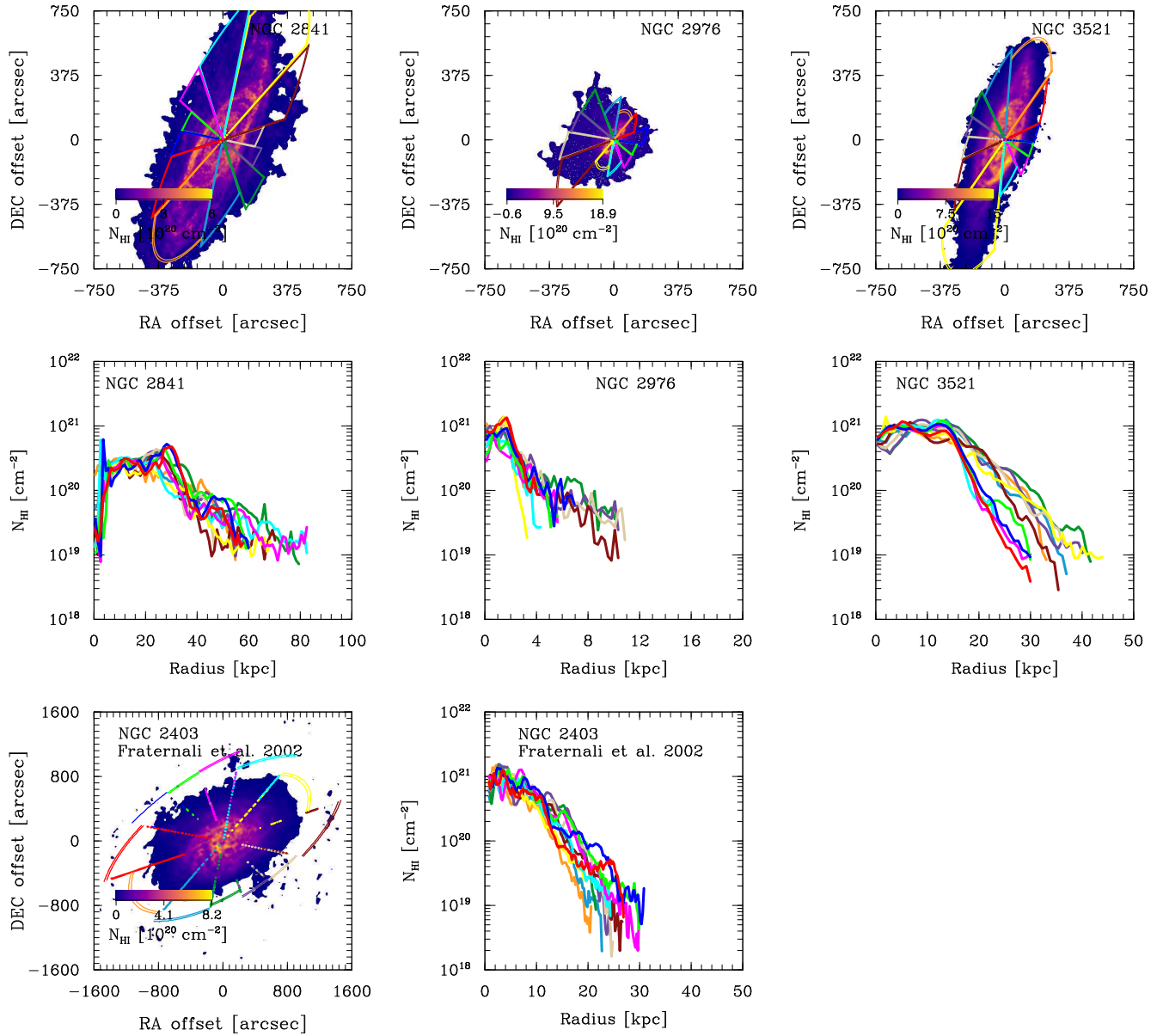


Figure B1. Continued.